The Mechanics of Metallic Folds

M.G. Walker, K.A. Seffen

Abstract: *We investigate the mechanical properties of metallic folds. In contrast to the common singular hinge assumption, we assume a finite geometry for the fold cross-section and consider the influence of the geometry on the mechanical behaviour. We derive the strain energy due to fold opening and show that reducing the size of the fold increases the energy required for fold opening and vice versa. In theory, as the fold size approaches the singular limit, the opening stiffness approaches infinity, but in practice this is limited by manufacturing constraints. Due to the large opening resistance of such folds, the deformation of origami structures made from folded metal will depend to a large extent on deformation of the panels. We consider a folded metallic strip with flexible panels manipulated by deformation at the panel edges, and identify the boundary between fold opening and panel bending dominated behaviour, which is confirmed by finite element analysis.*

1 Introduction

The increasing use of origami techniques in engineering applications has necessitated a shift away from paper-based materials to more robust metals and laminated composites. Folding paper locally tears fibres and, with repeated folding, gradually weakens the fold line, leading to eventual failure. In contrast, metal folding involves plastic deformation and work-hardening, where yield stresses in the fold robustly rise due to the forming process. Metal fold lines exhibit a typically high stiffness, which can subtract from the overall Origami character of the structure [Francis et al. 13].

The analysis of Origami structures has been dominated by two main techniques. The first assumes rigid plates connected by discrete fold lines, or 'rigid origami' [Evans et al. 15]. The folds themselves remain straight but accommodate relative rotations across them. Rigid folding this way can be described entirely by a kinematic analysis even if the fold lines are in some way stiff in practice; adding torsional springs along them does not affect the kinematic description. Example applications include deployable membranes for spacecraft [Miura 85], Origami-based robots [Felton et al. 14], metamaterials [Hawkes et al. 10], and medical stents [Kuribayashi et al. 06].

The second technique accounts for flexibility beyond the folds. For generality's sake, the fold line is treated as a general space curve connecting thin inextensible surfaces that can only bend [Duncan and Duncan 82, Dias and Audoly 14]. Differential geometry is then used to obtain the increase in strain energy due to defor-

mation of the panels, as well as the change in fold angle, if it has been modelled elastically. This technique is more complex which prevents its immediate application to large-scale origami structures with multiple folds.

In either case, the fold itself is modelled as a singular feature. The assumption that an elastic fold can be represented by a singular hinge with a well-behaved torsional spring has not been fully investigated. In this work, we investigate the mechanical properties of metallic folds for incorporation into the analysis of Origami structures.

Typical sheet metal folding processes create a constant curvature fold, and the formed radius and sector angle can be predicted using established formulae [Schey 00]. For this study we assume a finite geometry for the fold cross-section consisting of a uniform curvature cylindrical segment, in contrast to the common singular assumption. Using a linear elastic material model, we develop strain energy expressions for the opening of the fold and investigate the effect of the fold geometry on the opening behaviour of the cross-section.

Out-of-plane effects, such as flexure of the crease perpendicular to its axis, are not included in our analysis. We also assume that residual strains due to the forming process do not influence the elastic response. Our model is then used to find the fold opening elastic limit, which may be affected by residual strains, but we assume the cross-section is free from these effects here.

Due to the typically high opening stiffness of metallic folds, bending of the panels will have a significant influence on the behaviour of a folded sheet. We investigate how the fold and panel geometry influence the transition between fold opening dominated behaviour and panel bending dominated behaviour. Finally, we consider the analysis of a folded sheet with deformable panels opened by imposed displacements at the panel edges and compare the results to finite element analysis.

This study is principally concerned with folds in metallic materials. However, the results are also applicable to Origami structures made from other linear-elastic materials across a range of length scales, for example: nanoscale silicon [Malachowski et al. 14] and graphene [Miskin et al. 18]. The results will contribute to the understanding and design of Origami structures made using elastic materials.

2 Constant Curvature Thin Shell Fold

In the first instance, the cross-section of a fold with infinite axial depth is modelled as a constant curvature cylindrical segment of radius, r, and sector angle β, as shown in Fig. 1a. Because the depth is infinite, we may assume uniform axial behaviour governed by how the cross-section deforms. The fold has a uniform thickness, t, Young's modulus E, and Poisson's ratio ν. The fold thickness-to-radius ratio is assumed to be small enough for thin shell theory to apply.

To derive the strain energy per unit depth of fold due to compatible panel rotations, θ, on its edges, the deformed geometry, shown in Fig. 1b, is considered. The deformed fold is assumed to maintain a constant curvature, κ, since pure rotation is applied along its edges. This curvature is related to the edge rotation, θ, by ensuring compatibility of slope between the fold and the panel:

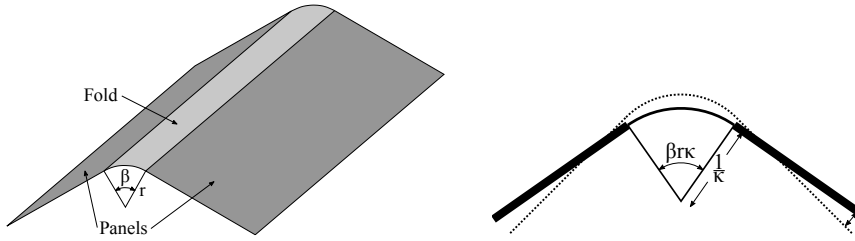

(a) *Undeformed* **(b)** *Deformed*

Figure 1: *Fold cross-section geometry in the undeformed (a) and deformed (b) states. The panels are considered as rigid plates; therefore only the fold region deforms.*

$$\kappa = \frac{2\theta}{\beta r} + \frac{1}{r} \tag{1}$$

The strain energy due to the edge rotation is obtained from the corresponding change in curvature and neglecting any axial deformation:

$$U_{Thin} = \frac{\beta r D}{2}\left(\kappa - \frac{1}{r}\right)^2 = \frac{2D}{\beta r}\theta^2 \tag{2}$$

where $D = Et^3/12(1-\nu^2)$ is the shell flexural rigidity. This only depends on the initial geometry of the fold and the edge rotations. As r approaches zero this energy approaches infinity; in reality this is limited by the onset of plastic deformations, as discussed in Section 4.

Large-radius folds (relative to thickness) can be used to accomodate the panel thicknes in 'thick' Origami [Chen et al. 15, Ku and Demaine 16]. In theory, when the fold radius $r > t/2$, the panels can be folded flat without interference at the fold. However, large-radius folds can result in additional degrees of freedom and more complex behaviour in practice [Peraza Hernandez et al. 17]. In this study only the opening behaviour of the fold is considered. Metallic folds are commonly made with a radius roughly equal to the thickness, where thin shell theory does not apply. To investigate this violation we consider a "thick" fold next.

3 Constant Curvature Thick Fold

For thick folds, the through-thickness radial stresses are no longer negligible. We resort to a continuum mechanics approach, where the fold is treated as a thick curved beam. The corresponding stress state from end moments (applied in our case by each panel to the fold edges) was derived by Timoshenko [Timoshenko and Goodier 51]. Assuming uniform deformed curvature, the end moments can be related to the change in fold curvature by: $M = Et^3(1/r - \kappa)/12$. The stress state

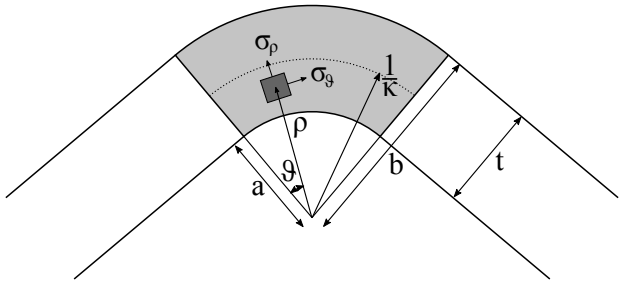

Figure 2: *Geometry of the thick fold model in addition to the geometry defined in Fig. 1, which applies along the neutral axis (shown dotted).*

can therefore be written as:

$$\sigma_\rho = \frac{Et^3}{3N}\left(\frac{1}{r}-\kappa\right)\left(\frac{a^2b^2\log\frac{b}{a}}{\rho^2}+a^2\log\frac{a}{\rho}+b^2\log\frac{\rho}{b}\right) \tag{3}$$

$$\sigma_\vartheta = \frac{Et^3}{3N}\left(\frac{1}{r}-\kappa\right)\left(-\frac{a^2b^2\log\frac{b}{a}}{\rho^2}+a^2\log\frac{a}{\rho}-a^2+b^2\log\frac{\rho}{b}+b^2\right) \tag{4}$$

$$\tau_{\rho\vartheta} = 0 \tag{5}$$

where ρ is a radial coordinate, ϑ is a circumferential coordinate, a is the inner radius, b is the outer radius, and κ is the deformed curvature of the fold at the neutral axis, see Fig. 2. Also,

$$N = \left(b^2-a^2\right)^2 - 4a^2b^2\log^2\left(\frac{b}{a}\right) \tag{6}$$

The strain energy of bending per unit depth into the page is obtained by integrating the strain energy density over the cross section, noting that the stresses do not depend on the circumferential coordinate ϑ:

$$U_{Thick} = \frac{\beta r\kappa}{2E}\int_a^b\left[\sigma_\vartheta^2+\sigma_\rho^2-2\nu\sigma_\vartheta\sigma_\rho\right]\rho\,\mathrm{d}\rho \tag{7}$$

$$= \frac{\beta r\kappa Et^6(b-a)(a+b)(\kappa-\frac{1}{r})^2}{36(1-\nu^2)N} \tag{8}$$

Substituting $a = 1/\kappa - t/2$, $b = 1/\kappa + t/2$, and Eqn 1 into Eqn 8, yields the strain energy due to an edge rotation, θ:

$$U_{Thick} = \frac{8Et^2\Phi^4\theta^2}{9\lambda(1-\nu^2)\left(\Phi^2-4\lambda^2\right)^2\log^2\left(\frac{2\lambda+\Phi}{2\lambda-\Phi}\right)-144\lambda^3\Phi^2} \tag{9}$$

where $\Phi = \beta + 2\theta$ is the deformed sector angle of the fold, and $\lambda = \beta r/t$ is the sector length-to-thickness ratio. In contrast to Eqn 2 for thin shells, the fold stiffness

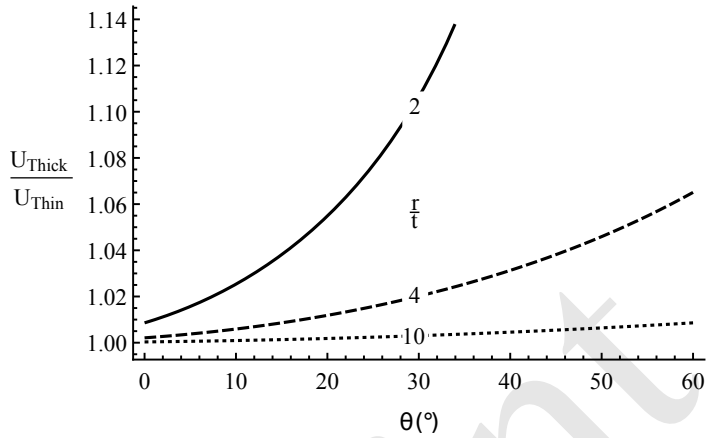

Figure 3: *Ratio of thick and thin fold strain energies, Eqn 9 and Eqn 2, for a fold with $\beta = 30^\circ$ and r/t ratios of* 2, 4, *and* 10. *For small values of r/t the thick fold model requires more energy to deform (it is stiffer). As the r/t ratio increases, the energy ratio approaches unity.*

here depends not only on the initial geometry of the fold, but also on the deformed fold sector angle, Φ. The logarithmic term in Eqn 9 imposes a restriction on the change in fold sector angle for the thick model:

$$\theta < \beta \left(\frac{r}{t} - \frac{1}{2} \right) \tag{10}$$

which is ultimately a restriction on the maximum deformed curvature: $\kappa < 2/t$, due to Eqn 1. Physically this limit represents a sheet folded back onto itself; therefore, a larger curvature is not physically possible.

The ratio of the thick fold energy, Eqn 9, to the thin fold energy, Eqn 2, is plotted in Fig. 3, where it approaches unity as r/t becomes large: a ratio of $r/t > 20$ is a commonly mentioned limit for thin shell behaviour, which works well in this case. The difference between the two energies also increases as the edge rotation, θ, increases. By repeating this calculation over a range of edge rotations, the difference between the two models was found to be less than 20% for moderate rotations.

4 Rotation Limits for Elastic Behaviour

The maximum circumferential stress in the thick fold model is obtained using Eqn 4, with $\rho = a$ for tension and $\rho = b$ for compression. These turn out to be equal in magnitude; setting the maximum tensile stress equal to the yield stress, σ_y, and solving for the edge rotation angle, we find at the onset of yielding:

$$\theta_y = \frac{3\beta\gamma\left(\left(1-4\gamma^2\right)^2\log^2\left(\frac{2\gamma-1}{2\gamma+1}\right)-16\gamma^2\right)}{16\gamma-4(2\gamma+1)^2\log\left(\frac{2\gamma+1}{2\gamma-1}\right)}\frac{\sigma_y}{E} \tag{11}$$

where $\gamma = r/t$, and the angle θ_y is assumed to be small. To test this assumption, consider a mild steel fold with $\gamma = 2$, a yield stress $\sigma_y = 200$ MPa, and elastic modulus $E = 200$ GPa. Using Eqn 11 results in $\theta_y = 0.0017\beta$, which is much less than unity for sector angles, $\beta < \pi$. For large γ, a good approximation of Eqn 11 is obtained using Eqn 1. Since the change in curvature is $\kappa - 1/r$, the fold rotation at yield for the thin shell model is: $\theta_y = \gamma\beta\sigma_y/E$; this is precisely the limit of Eqn 11 when γ becomes large.

The edge rotation angle at the onset of yielding is generally small for metallic materials. Therefore, elastic behaviour of the fold only occurs over a small range of rotations. Further opening of the fold will result in permanent plastic deformations.

The strain energy, and consequently the stiffness, of a fold increases as the size of the fold is reduced and, in the absence of plastic effects, theoretically approaches infinity as the fold radius is reduced to zero. As a result, deformation of the panel regions will have an important contribution to the mechanical behaviour of a folded sheet. The transition between fold opening and panel bending dominated behaviour is investigated in the next section.

5 Fold Geometry Limits for Origami Behaviour

Since the bending strain energy of either side panel is proportional to the shell flexural rigidity, D (units of N-m), and the fold opening energy is proportional to the fold opening stiffness (units of N), Lechenault et al. [F. et al. 14] propose that a natural length scale emerges from the ratio of these energies. They define this ratio as an Origami length scale, $L^* = 2D/k$, where k is the stiffness of the fold: for panel lengths much less than L^*, fold opening will dominate; while for lengths much larger than L^*, panel bending will dominate. Between these extremes both deformation mechanisms will be present.

The strain energy of opening was derived for thin shell folds in Section 2, and thick folds in Section 3. An equivalent, singular, torsional spring stiffness representing the opening behaviour of the discrete fold is obtained by comparing these energy expressions to the potential energy of a torsional spring: $\frac{1}{2}k\theta^2$, where k is the spring stiffness. Considering the thin shell energy in Eqn 2, the corresponding stiffness is therefore $4D/\beta r$. The Origami length scale of a thin shell fold is thus: $L^* = \beta r/2$. Similarly, using Eqn 9 for a thick fold:

$$L^* = \frac{3}{16\Phi^4}\left[16\lambda^2\Phi^2-\left(\Phi^2-4\lambda^2\right)^2\log^2\left(\frac{2\lambda+\Phi}{2\lambda-\Phi}\right)\right]\frac{\beta r}{2} \tag{12}$$

which approaches the thin shell Origami length scale, $L^* = \beta r/2$, for large γ (note: $\lambda = \beta r/t = \beta\gamma$). On the other hand, Eqn 12 reduces to $L^* = 3\beta r/8$ for the minimum value of γ equal to one half.

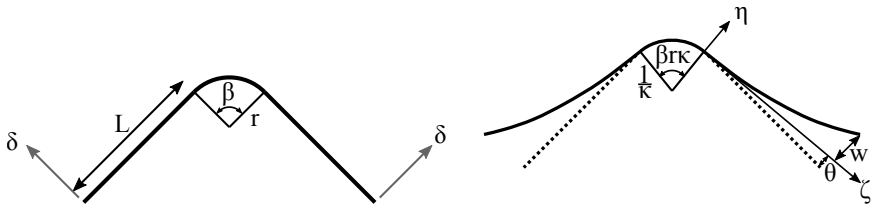

(a) *Undeformed* **(b)** *Deformed*

Figure 4: *Cross-section geometry for a folded strip with deformable panels in the undeformed (a) and deformed (b) states. A displacement of* $\delta = w + L\sin\theta$ *is imposed perpendicular to the panel which opens the strip by a combination of panel bending and fold opening.*

6 Analysis of a Folded Strip with Flexible Panels

The undeformed cross-section of a folded strip is shown in Fig. 4a. The fold has the same geometry as shown in Fig.1 and the panels each have a length of L. The folded strip is assumed to be infinite in depth as before. We consider the opening action caused by a displacement δ imposed at the free panel edges, without reference to the forces which cause such a displacement. Both the panel and the fold deform as a result of this displacement. The η-ζ coordinate system of the panel is located at the connection between the fold and the panel, as shown in Fig. 4b. Under deformation the fold edges rotate by θ, and the ζ axis remains oriented along the fold tangent at the fold-panel interface. The panel itself deforms relative to the ζ axis by a displacement, w, at the free panel edge. These deformations sum to to the total imposed displacement $\delta = L\sin\theta + w$.

Considering the deformation of the panels, the governing equation of the deformation of a thin plate is given by:

$$D\frac{d^4\eta}{d\zeta^4} = 0 \tag{13}$$

The boundary conditions for the panel enforce compatibility at the fold-panel interface through:

$$\frac{d\eta}{d\zeta} = 0 \qquad\qquad \eta = 0 \tag{14}$$

and the boundary conditions at the free edges are:

$$\frac{d^2\eta}{d\zeta^2} = 0 \qquad\qquad \eta = w \tag{15}$$

The deformed panel shape is thus solved as:

$$\eta(\zeta) = \frac{w\zeta^2(3L-\zeta)}{2L^3} \tag{16}$$

and the total strain energy per unit depth due to bending of a single panel is:

$$U_P = \frac{D}{2}\int_0^L \left(\frac{d^2\eta}{d\zeta^2}\right)^2 d\zeta = D\frac{3w^2}{2L^3} \tag{17}$$

The energy of deformation of the fold region, U_B, is given in Eqns 2 or 9, depending on the r/t ratio, resulting in a total energy of deformation of:

$$U = 2U_P + U_B \tag{18}$$

which depends on two parameters, w and θ, and the initial geometry.

For a particular displacement $\delta = L\sin\theta + w$, we find after substitution, for the thin shell fold:

$$U = D\left[\frac{3(\delta - L\sin\theta)^2}{2L^3} + \frac{2\theta^2}{\beta R}\right] \tag{19}$$

The angle, θ, corresponding to the displacement, δ, is found by minimising the total strain energy. For the thin shell fold:

$$\theta_{\text{Thin}} = \frac{3\Delta\mu}{3\mu + 2} \tag{20}$$

where $\mu = \beta r/L$ and $\Delta = \delta/L$. For the thick fold we find:

$$\theta_{\text{Thick}} = \frac{9\Delta\mu\left[\left(1-4\gamma^2\right)^2\log^2\left(\frac{2\gamma+1}{2\gamma-1}\right) - 16\gamma^2\right]}{9\mu\left(1-4\gamma^2\right)^2\log^2\left(\frac{2\gamma+1}{2\gamma-1}\right) - 16\left(9\gamma^2\mu + 2\right)} \tag{21}$$

where it can be confirmed that as γ becomes very large, θ_{Thick} approaches θ_{Thin}. The ratio of the fold energy to the panel energy, for the thin shell fold, is now:

$$\frac{U_{\text{Thin}}}{U_{\text{Panel}}} = \frac{6\Delta^2\mu}{(3\mu+2)^2\left[\Delta - \sin\left(\frac{3\Delta\mu}{3\mu+2}\right)\right]^2} \tag{22}$$

Equation 22 has a weak dependence on Δ for realistic values of μ and Δ where $\mu\Delta \ll 1$. An equivalent, but lengthy, expression is obtained in the same manner for the thick fold case, which depends on the ratios, r/t and L/t. As these ratios become very large the fold-to-panel energy ratio approaches Eqn 22. The ratio of the thick fold to panel energies is a minimum when $r/t = 0.5$ and $L/t \to \infty$, which returns after some algebra:

$$\frac{72\Delta^2\mu}{(9\mu+8)^2\left[\Delta - \sin\left(\frac{9\Delta\mu}{9\mu+8}\right)\right]^2} < \frac{U_{\text{Fold}}}{U_{\text{Panel}}} < \frac{6\Delta^2\mu}{(3\mu+2)^2\left[\Delta - \sin\left(\frac{3\Delta\mu}{3\mu+2}\right)\right]^2} \tag{23}$$

Equation 23 is plotted in Fig. 5. When $L/\beta r$ lies below $L^*/\beta r = 0.5$, the fold deformation energy increases rapidly in comparison to the panel energy. Above $L^*/\beta r = 0.5$, the rate of decrease of the energy ratio decreases. As $L/\beta r \to \infty$ the panel energy dominates and the energy ratio approaches zero.

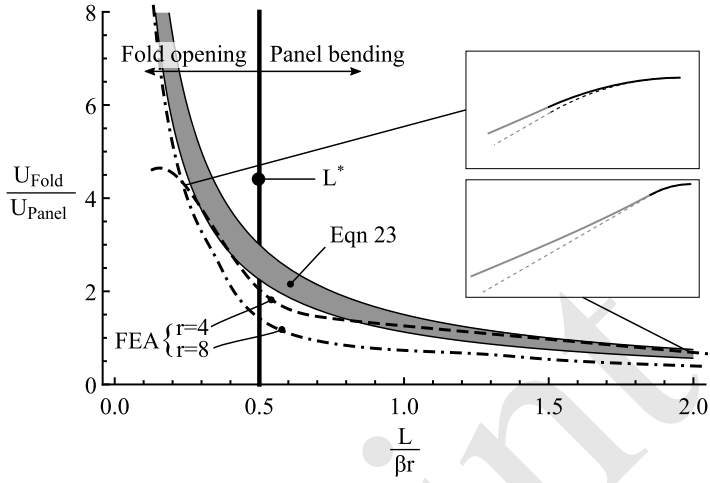

Figure 5: *Ratio of fold strain energy to panel strain energy for the boundary cases in Eqn 23, for* $\Delta = \delta/L = 0.01$. *Results from the finite element analysis study are also shown for strips with* $\beta = 60^\circ$, $t = 0.5$, $r = 4$ *and* $r = 8$. *The insets show the deformed cross-section (solid) compared to the initial cross-section (dashed) for the finite element model. The origami length scale,* L^*, *provides a good measure of the transition between fold bending dominated behaviour and panel bending dominated behaviour.*

7 Finite Element Analysis

A finite element study was performed using ABAQUS [Systèmes 14] to evaluate the analytical prediction. The cross-section was modelled as shown in Fig. 4a, with a sector angle $\beta = 60^\circ$, a thickness of 0.5 mm, and a linear elastic material model with Young's modulus $E = 200$ GPa and Poisson's ratio $\nu = 0.3$. Reduced integration, four-noded thin shell elements, S4R, were used, all degrees of freedom at the centreline of the fold were fixed and a non-linear static analysis was performed in half symmetry. A displacement of $\delta = 0.01L$ was imposed at the panel edge perpendicular to the initial panel inclination, an angle of $\beta/2$ to the vertical.

The fold to panel energy ratios, for fold radii of 4 mm and 8 mm, are included in Fig. 5. The shape of the curves follow Eqn 23 well but lie slightly below. One reason is Eqn 23 assumes a constant fold curvature; the stretching energy is also neglected. The finite element results also show a small dependence on the initial fold radius, r, which is not present in Eqn 23.

The predicted Origami length, L^*, provides a good indication of the transition between fold opening and panel bending dominated behaviour for both the analytical model as well as the finite element results. For a constant thickness strip, the deformation behaviour is a combination of panel bending and fold opening, except when the panel length is very long, or very short, in comparison to the fold sector arc-length.

8 Conclusions

This study considered the cross-sectional deformation mechanics of a fold with a discrete shape consisting of a constant curvature cylindrical segment. The strain energy due to the opening of this fold was derived using both a thin shell approach and a continuum mechanics approach. The thin shell approach is applicable when the fold radius-to-thickness ratio is greater than about 20. Below this limit, the thin shell assumptions are increasingly violated and the latter approach is appropriate. In either case, if plasticity is neglected, the stiffness (and energy) approaches infinity as the fold radius is reduced to zero.

Simple design rules were developed for the fabrication of metallic Origami structures. The fold opening limit for elastic behaviour was derived and found to be $\theta_y = r\beta\sigma_y/Et$ for thin folds. For thicker folds, the more complex expression in Eqn 11 must be used. Because folds in metals are typically small, they have a high bending stiffness in comparison to the panels. The panel length where the opening of a folded sheet transitions between fold opening dominated to panel bending dominated behaviour was shown to be one half of the fold sector length, $L^* = \beta r/2$, for thin folds. For thick folds this decreases to $L^* = 3\beta r/8$.

The relative deformation of the fold and panel regions, under imposed displacement at the panel edges, was considered in detail using an energy approach and compared to finite element analysis, showing excellent agreement. The results also showed that the Origami length, L^*, provides a good indication of the dominant deformation mode. The results of this study will be useful for the design and analysis of Origami structures made from folded metal and other linear-elastic materials.

References

[Chen et al. 15] Y. Chen, R. Peng, and Z. You. "Origami of thick panels." *Science* 349:6246 (2015), 396–400. doi:10.1126/science.aab2870.

[Dias and Audoly 14] M.A. Dias and B. Audoly. "A non-linear rod model for folded elastic strips." *Journal of the Mechanics and Physics of Solids* 62 (2014), 57–80. doi:10.1016/j.jmps.2013.08.012.

[Duncan and Duncan 82] J.P. Duncan and J.L. Duncan. "Folded developables." *Proceedings of the Royal Society of London A* 383 (1982), 191–205.

[Evans et al. 15] T.A. Evans, R.J. Lang, S.P. Magleby, and L.L. Howell. "Rigidly foldable origami gadgets and tessellations." *Royal Society Open Science* 2:9 (2015), 150067. doi:10.1098/rsos.150067.

[F. et al. 14] Lechenault F., B Thiria, and M. Adda-Bedia. "Mechanical response of a creased sheet." *Physical Review Letters* 112:24 (2014), 244301. doi:10.1103/PhysRevLett.112.244301.

[Felton et al. 14] S. Felton, M. Tolley, E. Demaine, D. Rus, and R. Wood. "A method for building self-folding machines." *Science* 345:6197 (2014), 644–646. doi:10.1126/science.1252610.

[Francis et al. 13] K.C. Francis, J.E. Blanch, S.P. Magleby, and L.L. Howell. "Origami-like creases in sheet materials for compliant mechanism design." *Mechanical Sciences* 4:2 (2013), 371–380. doi:10.5194/ms-4-371-2013.

[Hawkes et al. 10] E. Hawkes, B. An, N. M. Benbernou, H. Tanaka, S. Kim, E. D. Demaine, D. Rus, and R. J. Wood. "Programmable matter by folding." *Proceedings of the National Academy of Sciences* 107:28 (2010), 12441–12445. doi:10.1073/pnas.0914069107.

[Ku and Demaine 16] Jason S. Ku and Erik D. Demaine. "Folding flat crease patterns with thick materials." 8:June 2016 (2016), 1–6. doi:10.1115/1.4031954.

[Kuribayashi et al. 06] Kaori Kuribayashi, Koichi Tsuchiya, Zhong You, Dacian Tomus, Minoru Umemoto, Takahiro Ito, and Masahiro Sasaki. "Self-deployable origami stent grafts as a biomedical application of Ni-rich TiNi shape memory alloy foil." *Materials Science and Engineering A* 419:1-2 (2006), 131–137. doi:10.1016/j.msea.2005.12.016.

[Malachowski et al. 14] Kate Malachowski, Mustapha Jamal, Qianru Jin, Beril Polat, Christopher J. Morris, and David H. Gracias. "Self-folding single cell grippers." *Nano Letters* 14:7 (2014), 4164–4170. doi:10.1021/nl500136a.

[Miskin et al. 18] Marc Z. Miskin, Kyle J. Dorsey, Baris Bircan, Yimo Han, David A. Muller, Paul L. McEuen, and Itai Cohen. "Graphene-based bimorphs for micron-sized, autonomous origami machines." *Proceedings of the National Academy of Sciences* 115:3 (2018), 201712889. doi:10.1073/pnas.1712889115.

[Miura 85] K. Miura. "Method of packaging and deployment of large membranes in space." Technical report, Institute of Space and Astronautical Science, 1985.

[Peraza Hernandez et al. 17] E.A. Peraza Hernandez, D.J. Hartl, and D.C. Lagoudas. "Design and simulation of origami structures with smooth folds." *Proceedings of the Royal Society A: Mathematical, Physical and Engineering Science* 473:2200 (2017), 20160716. doi:10.1098/rspa.2016.0716.

[Schey 00] J.A. Schey. *Introduction to Manufacturing Processes*, Third edition. McGraw-Hill, 2000.

[Systèmes 14] Dassault Systèmes. *Abaqus Theory Guide*, 2014.

[Timoshenko and Goodier 51] S. Timoshenko and J.N. Goodier. *Theory of Elasticity*, Second edition. London: McGraw-Hill, 1951.

Martin G. Walker
Mary Ewart Junior Research Fellow, Somerville College and Department of Engineering Science, University of Oxford, Woodstock Road, Oxford, OX2 6HD
e-mail: martin.walker@some.ox.ac.uk

Keith A. Seffen
Reader in Structural Mechanics, Department of Engineering, University of Cambridge, Trumpington Street, Cambridge, CB2 1PZ
e-mail: kas14@eng.cam.ac.uk